Journal of King Saud University – Science 34 (2022) 101836

Contents lists available at ScienceDirect

Journal of King Saud University – Science

journal homepage: www.sciencedirect.com

Original article

# Petrology and kinematic vorticity constraints of the Al Amar region, Northern Ar-Rayn terrane, Eastern Arabian shield, Saudi Arabia

Hussain J. Al Faifi [a,*], Lami Mohammed [a,b], Abdel Aziz Mohamed Al Bassam [a], Osama M.K. Kassem [c]

[a] Geology and Geophysics Department, Faculty of Science, King Saud University, Riyadh 11451, Saudi Arabia
[b] Department of Geology, Faculty of Science, Taiz University, Taiz, Yemen
[c] Department of Geology, National Research Center, Al-Behoos Str., 12622 Dokki, Cairo, Egypt

ARTICLE INFO

*Article history:*
Received 17 June 2021
Revised 16 December 2021
Accepted 12 January 2022
Available online 20 January 2022

*Keywords:*
Petrology
Kinematic analysis
Al Amar region
Ar-Rayn terrane
Arabian Shield

ABSTRACT

The Neoproterozoic basement rocks in Ar Rayn terrane set as parts in the Eastern Arabian Shield. It focus the petrological and kinematic vorticity for high deformed volcanic and granitoids rocks in the Al-Amar locality. The volcanic rocks divide into two main series, the eastern sequence cycle represents dacite, rhyodacite, rhyolite and ignimbrites, and the western sequence cycle characterizes andesite and pyroclastics. Furthermore, the granitoids rocks content monzodiorite, tonalite, granodiorite and alkali-feldspar granite. For assessing the proportions of pure and simple shear contributions in penetrative deformed rocks, the kinematic vorticity number (Wm) to the mean appreciation by applying porphyroclast, rotating in a flowing matrix is crucial. In the Ar Rayn terrane of Arabian shield, kinematic vorticity numbers for high deformed metavolcanics and granitoids gneisses vary from 0.4 to 0.6. The deformation in the studied area varied from simple shear, according to vorticity and strain studies. Nappe stacking getting ready during the thrusting activity only through the Al Amar –Idsas fault, according to the results, most likely due to brittle imbrication. A penetrative sub-horizontal foliation formed sub-parallel to the nappe contacts with the beneath laying nappes, showing that the ductile strain was superimposed on the construction of the nappe under high pressure. The Ar Rayn terrane was created sub-horizontal foliation by the buildup of ductile strain during under plating, which was induced by a vertical shortening component. This foliation was formed in the majority of cases during the thrusting nappes upon each other, implying that nappe stacking was related to vertical shortening due to a massive scale by the active Al Amar –Ideas fault.


## 1. Introduction

The Arabian Shield (AS) is mainly consisting of Neoproterozoic basement rocks for Ediacaran arc that created in the ocean of Mozambique, which opened during Rodinia's middle Neoproterozoic break-up. The collision of East and West Gondwana produced the supercontinent Gondwana (Meert and Torsvik 2003; Stern 1994). The Pan-African Orogeny, which occurred end of the Neoproterozoic period, was buildup by this massive collision (Johnson et al., 2013). The Mozambique Belt was formed by remobilizing Mozambique and Madagascar. The Mozambique Belt's crust differs significantly from the Arabian-Nubian Shield (ANS), which is typically "juvenile" crust created by partial melting the mantle of the Earth (Johnson et al., 2013).

According to several authors, the Arabian Shield went through numerous stages in its evolution to its current condition and the break-up of Rodinia during the middle Neoproterozoic are depicted. Also the opening and closing of a wide "Mozambique Ocean" with associated formation of juvenile crust. Continued convergence and tectonic escape when continental fragments from east and west Gondwana collide (Stern 1994). The end of Neoproterozoic time, a new supercontinent "Greater Gondwana" came into existence. It's possible that most of the crust that currently underlies the Arabian Peninsula has shifted northward. The geological units of Arabian Shield are made up of bedded volcanosedimentary and volcanic rocks (Johnson et al. 2013). Regional orogenic motions, accompanied by plutonic rocks of varying size and shape. Also, they influenced the composition of intrusive and volcanic rocks. Metamorphism and crystallization of ancient rocks

* Corresponding author.
*E-mail address:* hualfaifi@KSU.EDU.SA (H.J. Al Faifi).
Peer review under responsibility of King Saud University.

Production and hosting by Elsevier

https://doi.org/10.1016/j.jksus.2022.101836
1018-3647/

originated through tectonic deformation, resulting in bedded metamorphic rocks like green schist facies (Doebrich et al. 2004).

The Arabian Shield is predominantly based on two types of rocks (Fig. 1). Bedded are the first rock types, which were deposited in layers and encompass all forms of clastic sedimentary and extrusive rocks. Also, the second one is intruded intrusive bodies, which are incorporated in bedded rocks and characterise a significant region of the Arabian Shield. The Al Amar-Idsas is a suture zone having a 200-kilometer apparent length and a 6-kilometer apparent width (Fig. 1). It was thought to be located between two terranes: an eastern terrane (island arc) with a volcanic sequence known as the Ar Rayn terrane, and a western terrane known as

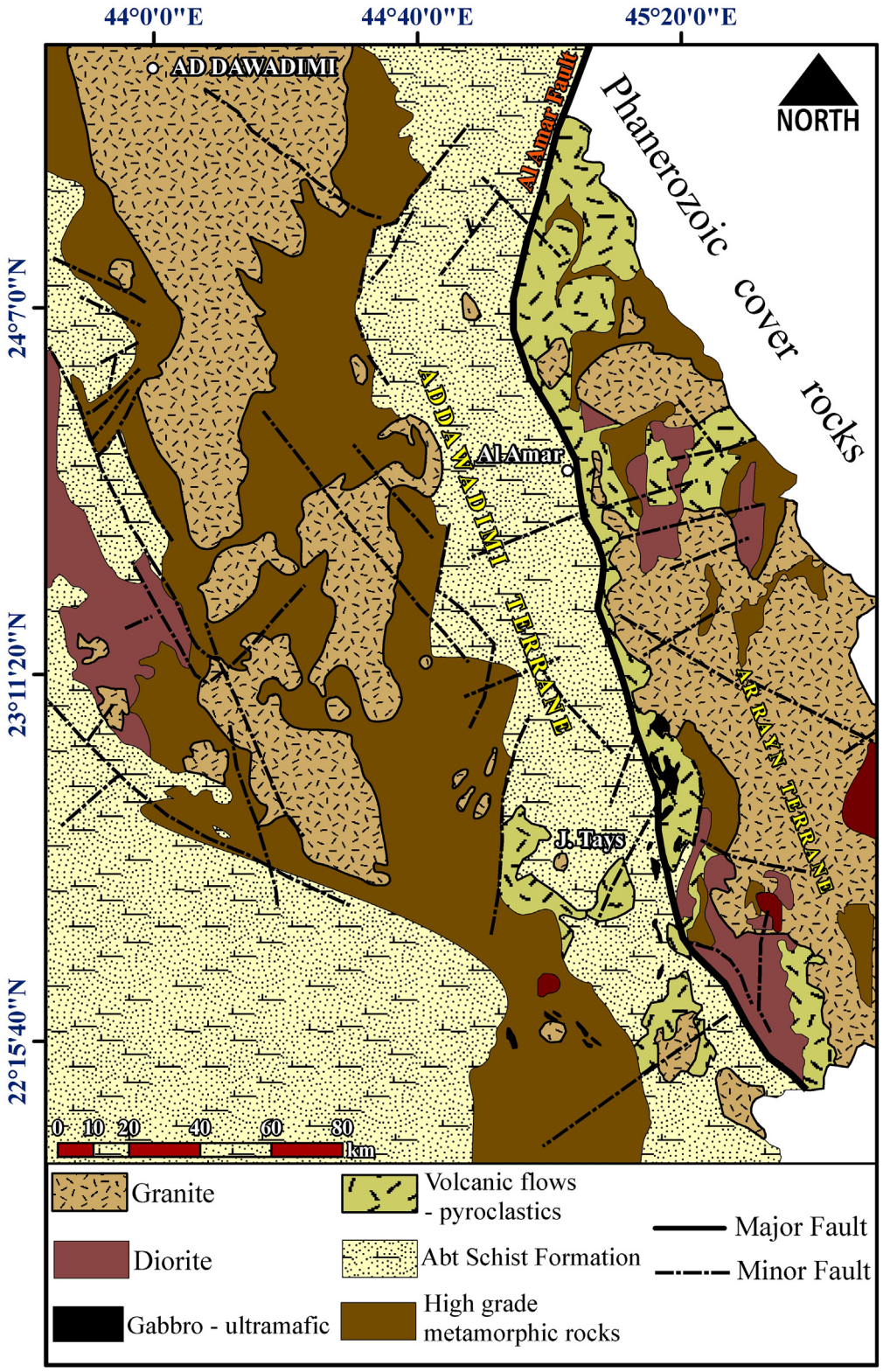


**Fig. 1.** Geologic map of the Ar Rayn terrane and Ad Dawadimi terrane.

the Ad Dawadimi terrane, which contains siltstone and mudstone originated an oceanic trench characterized by low metamorphic grade for chlorite schist rocks (Fig. 1).

The studied area is located in the western of the Ar Rayn region, and the present work examined the impact of various combinations of simple and pure shears, object aspect ratio, and matrix rheology (Fig. 2). In metavolcanic rocks and deformed granitiods, it also results in flow disruption on the development of shape-preferred orientation of a population of rigid grains during progressive deformation. The shearing must be studied in the form of finite strain ellipsoid and flow path analysis. Strain ratios are significant in a variety of applications, such as Rf/ and Fry techniques. Absolute strains are necessary in order to detect pre-deformation item sizes. In other circumstances, strain ratios may also be known if the rocks have objects of known form or distribution. As part of a measuring strain method, deformed rocks were employed (Kassem and Ring 2004; Ring and Kassem 2007; Kassem and Abd El Rahim, 2010; Kassem et al., 2019a,b; Lami et al., 2020). The research focuses on elucidating orogenic phases during nappe formation, as well as petrographic and microstructural examination of the Al Amar region, as well as detecting rigid object orientation during progressive deformation. The goal of this research is to elucidate the Al Amar region's tectonic evolution.

## 2. Geological setting

In the Arabian Shield, Ar-Rayn terrane formation is common in Ediacaran post-amalgamation basins, deposited on local and regional unconformities formed on arc assemblages in the basement rocks. Close to or directly along the strike-slip faults in the eastern Arabian Shield zones associated with Orogen-normal shortening and suturing, the basins of the Al Amar group are occupied with volcanoclastic and volcanic rocks (Johnson et al., 2013).

The present area is situated in the Ar Ryan terrane, which at least an area between the terranes in the eastern edge of Arabian Shield, and separates the territory of religion and Dawadimi what is known Al Amar suture, so that the eastern of which the board encloses a volcanic succession followed by the Al Amar group, while containing Western ones are the Abt Schist Formation (Fig. 2). The Al Amar area covers the Ar Rayn Terrane's eastern edge, which is situated to the east of the Arabian Shield. Andesite, rhyolite, and pyroclastic rocks composed primarily in the Al Amar

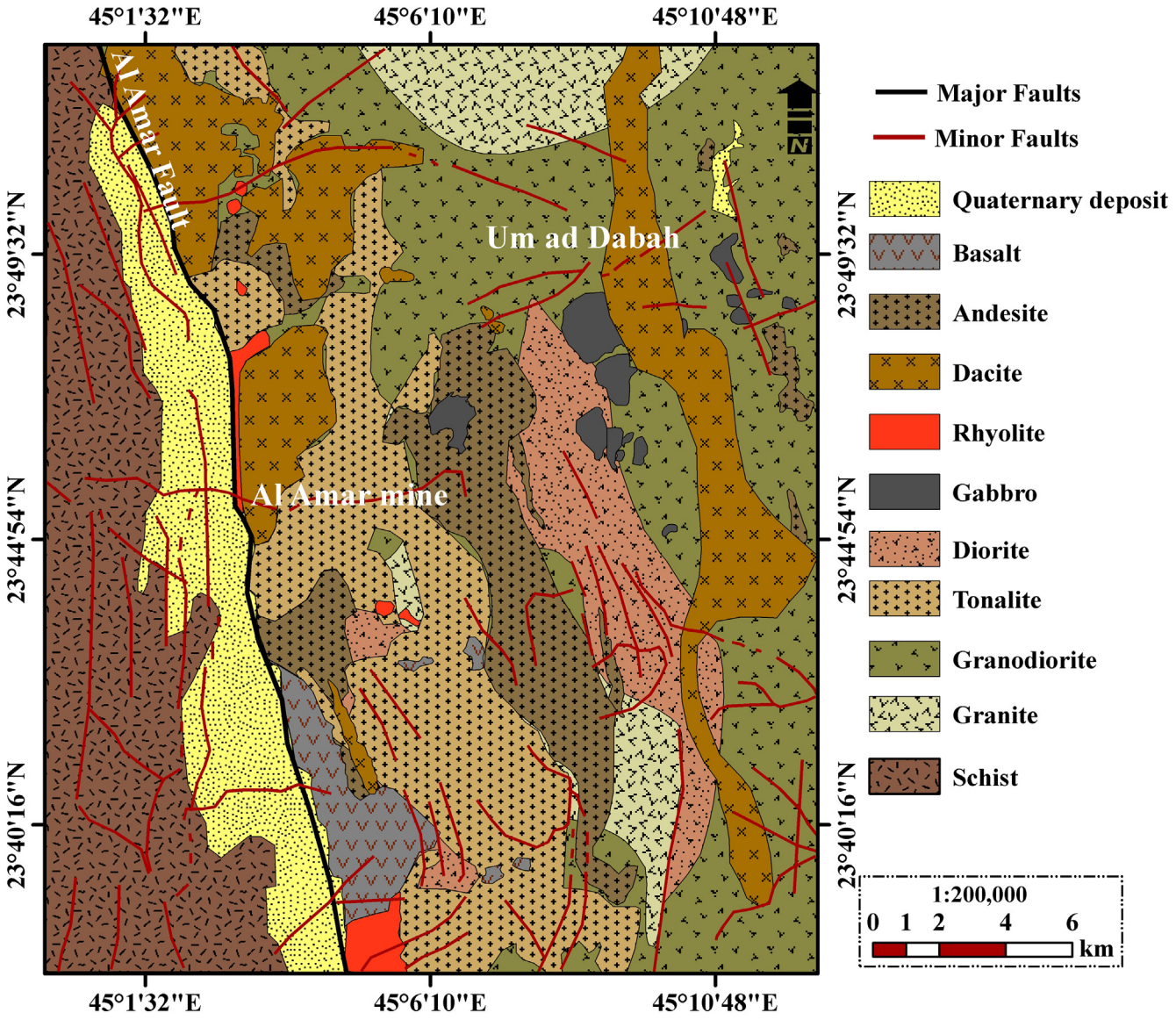


**Fig. 2.** Geologic map for North Ar Ryan terrane.

group. In addition, it consists of para-gneiss and meta granite (gneissose granite). Synorogenic tectonics including folding and faulting, and also ongoing volcanic activity and intrusion body, had an impact.

The Neoproterozoic rocks have volcanic arc complex with three separate suites of intrusive rocks that have all experienced low-grade greenschist metamorphism (Doebrich et al., 2007a). The arc assemblages include juvenile suites of calc-alkaline and tholeiitic volcanic rocks, large quantities of volcanic rocks, and also tonalite-trondhjemite type intrusions and diorite – granodiorite intrusion body (Doebrich et al., 2007a). The last Neoproterozoic in the eastern Arabian shield, according to Doebrich et al. (2007b), is characterised by arc formation and accretionary events around 620–600 Ma. Tectonic evaluation in the Ar-Rayn terrane took occurred around the northeastern border of the East African orogeny through the last phases of the Supercontinent Gondwana. Doebrich et al. (2007b) classified the Al Amar group rocks into two types: metamorphosed eastern series and less metamorphosed western series (Fig. 2). The Al Amar group's eastern and western sequences contain rocks ranging in composition from basalt to rhyolite. Also, Doebrich et al. (2007b) abandoned the eastern and western sequence terms and separated the Al Amar group rocks into two units that were more well characterised. The eastern sequence mainly overlies the western sequence. Volcanic basaltic, volcaniclastic and andesitic rocks with secondary siltstone and marble make up the western succession. In addition, felsic volcanic and volcaniclastic rocks (rhyolite and dacite flows, and also tuffs and ignimbrites with interlayered carbonate rocks) are established in the eastern sequence. According to Vaslet et al. (1983), the volcanic arc evolved in a changing shallow marine and subaerial environment.

## 3. Techniques and sampling

Using finite strain and kinematic vorticity analysis have investigated sheared metavolcanics, metasedimentary, Abt schist and gneisses rocks revealed feldspar and quartz crystals, in addition to mafic crystals, for the basement rocks in the Ar Rayn terrane (Ramsay 1967; Fry 1979; Ramsay and Huber 1983; Kassem, 2011; Kassem et al., 2012; Kahal et al., 2019). Using the Rf/φ and Fry methods to demonstrate the distinction between felsic and mafic minerals (Ramsay and Huber, 1983), felsic minerals were measured independently from mafic minerals due to different physical parameters and metamorphic conditions (Passchier and Trouw 1995). To prepare samples, thin sections were cut along three mutually perpendicular planes subparallel to the XY, YZ, and XZ main planes. Measurements on XY, XZ, and YZ sections were made in order to identify the three-dimensional strain geometry. The RJH Strain Calculator 3.1 application (https://www.holcombe.net.au/software/straincalculator.html), which permits different parameters to be inserted, was used to calculate and visualise the strain results.

Rotated rigid objects (Passchier, 1987), deformed vein sets (Passchier, 1990), the rotation of material lines and stretch (Passchier and Urai, 1988), and the kinematic vorticity number (Wm) has been calculated using curving fibres round feldspar and quartz objects (Ring and Brandon, 1999). The equations regulating rigid objects rotation in a viscous medium flowing were utilized to measure the degree of non-axial from rotating rigid objects (Ghosh and Ramberg, 1976; Passchier, 1987). The sensation and a particle's rate of rotation are impacted by axial ratio (R), orientation, and the proportion of shear strain to shear elongations in the shear plane, as demonstrated by Ghosh and Ramberg (1976). As even the shear strain grows and the rate of stretching equals the rate of rotation for Wm = 1, i.e. simple shear, all objects that act as active markers with Rc will rotate independently. If Wm is less than 1, shearing includes a component of pure shear (Simpson and De Paor 1993: general or sub-simple shear), then the rotation of particles with increasingly decreasing aspect ratios is suppressed. Not all objects are free to spin continuously for any fluid flow with Wm < 1. Particles having an aspect ratio greater than a particular value, Rc, will spin until they find a stable orientation. Rotation is permitted for aspect ratios smaller than the crucial value. The Rc value, which distinguishes freely spinning particles from those that have stabilized their orientation, is a meaning of non-axial degree (Passchier 1987):

$$\mathrm{Wm} = \left(\mathrm{R}_c^2 - 1\right)/\left(\mathrm{R}_c^2 + 1\right)$$

According to Passchier (1987), the sample should meet five main criteria: a) homogeneous deformation linked to the sample's scale, b) identifying the difference in grain size between the rigid grains and the matrix, c) strong finite strain, d) the rigid grains are near the orthorhombic shape, and e) a large number of rigid grains. To determine the degree of non-coaxiality in a rotational rigid ellipsoid, the study performed two approaches (Rigid Grain Net (RGN) and Passchier). Data may be put into an Excel worksheet while on the microscope and plotted immediately on an RGN that is used as a chart basis in Excel, which is a major advantage of utilizing the RGN. Rigid object rotation is employed by the primary computations of a flowing viscous media in the Passchier technique (Passchier, 1987; Law et al, 2004; Jessup et al., 2007; Zhang and Fossen 2020).

Our briefly microscopic work described about 80 thin sections, which illustrated the various types of rocks measurements, also, the petrography of the major lithological rocks units show representative assemblages and textures. Thirty-four rock samples were collected from studied area. Ten samples symbolized metavolcanics rocks (meta-dacite, meta-rhyolite, and meta-andesite). Fourteen samples represented intrusive rocks (such as tonalite, granodiorites, alkali feldspar granite, diorite and gneisses). Ten samples represented Abt schist rocks. All collected samples were investigated the kinematic vorticity, finite strain and petrography during the fieldwork and laboratory (Table 1).

## 4. Results

### 4.1. Petrography

The Al Amar group rocks defined to the metavolcanics rocks subdivide into more clearly defined two units. The eastern sequence mainly overlies the western sequence. The western sequence consists of volcanic basaltic, andesitic rocks and volcaniclastic rocks with subordinate marble and siltstone. As well, the eastern sequence comprises felsic volcaniclastic and volcanic rocks dacite flows and rhyolite, and also tuffs and ignimbrites with interlayered carbonate rocks. In the eastern sequence cycle, rhyolite is composed of K-feldspar and quartz with varying quantities of phenocrysts embedded in a microcrystalline groundmass (Fig. 3A). Dacite represents mainly by tabular phenocrysts of plagioclase, quartz and altered mafic (Fig. 3B). Ignimbrite consists of crystals and crystal fragments of plagioclase, K-feldspar and quartz associated with pumice fragments, glass shards and lithic fragments (Fig. 3C). In the western sequence cycle, andesite represents massive, fine-grained and greenish grey in color with opaque minerals and sericite (Fig. 3D). Pyroclastics mostly created of crystal particles, crystal tuffs and volcanic breccia, with lithic and ash tuffs thrown in for good measure (Fig. 3E). Listwanite represents mainly patches and masses within the Al Amar region surrounding the magnesite or carbonate crystals, antigorite produces a mesh structure of tiny flakes (Fig. 3F).

**Table 1**
Finite strain data for collected samples from Al Amar area.

| .Sample No | Rock Type | Methods | SX | SY | SZ | RXY | RYZ | RXZ | Rc | Wm | K | R | LogX/Y | Log Z/Y | Nadi strain | Lode's |
|---|---|---|---|---|---|---|---|---|---|---|---|---|---|---|---|---|
| **AR1** | **Abt Schist** | **Rf/φ** | 1.42 | 1.14 | 0.62 | 1.25 | 1.85 | 2.31 | 2.6 | 0.52 | 0.29 | 2.1 | 0.1 | −0.27 | 0.613 | 0.473 |
| | | **Fry** | 1.73 | 0.85 | 0.68 | 2.03 | 1.25 | 2.54 | | | 4.13 | 2.28 | 0.31 | −0.1 | 0.688 | 0.521 |
| **AR2** | **Abt Schist** | **Rf/φ** | 1.56 | 1.07 | 0.6 | 1.45 | 1.8 | 2.62 | … | … | 0.56 | 2.25 | 0.16 | −0.26 | 0.686 | 0.224 |
| | | **Fry** | 1.69 | 1.4 | 0.42 | 1.2 | 3.33 | 4 | | | 0.09 | 3.53 | 0.08 | −0.52 | 1.065 | 0.735 |
| **AR3** | **Abt Schist** | **Rf/φ** | 1.57 | 1.06 | 0.6 | 1.48 | 1.76 | 2.6 | … | … | 0.64 | 2.23 | 0.17 | −0.24 | 0.678 | 0.179 |
| | | **Fry** | 1.65 | 1.03 | 0.59 | 1.61 | 1.75 | 2.81 | | | 0.81 | 2.36 | 0.21 | −0.24 | 0.731 | 0.083 |
| **AR4** | **Abt Schist** | **Rf/φ** | 1.42 | 1.42 | 0.5 | 1.01 | 2.86 | 2.87 | 2.5 | 0.6 | 0.01 | 2.86 | 0 | −0.46 | 0.859 | 0.989 |
| | | **Fry** | 1.85 | 0.99 | 0.54 | 1.86 | 1.83 | 3.4 | | | 1.03 | 2.69 | 0.27 | −0.26 | 0.865 | −0.012 |
| **AR5** | **Abt Schist** | **Rf/φ** | 1.38 | 1.23 | 0.59 | 1.12 | 2.09 | 2.34 | … | … | 0.11 | 2.21 | 0.05 | −0.32 | 0.653 | 0.727 |
| | | **Fry** | 1.66 | 0.88 | 0.69 | 1.89 | 1.27 | 2.4 | | | 3.3 | 2.16 | 0.28 | −0.1 | 0.64 | −0.454 |
| **AR6** | **Abt Schist** | **Rf/φ** | 1.37 | 1.12 | 0.65 | 1.22 | 1.73 | 2.12 | … | … | 0.31 | 1.95 | 0.09 | −0.24 | 0.548 | 0.459 |
| | | **Fry** | 1.28 | 1.26 | 0.62 | 1.01 | 2.04 | 2.06 | | | 0.01 | 2.05 | 0 | −0.31 | 0.586 | 0.973 |
| **AR7** | **Abt Schist** | **Rf/φ** | 1.33 | 1.14 | 0.65 | 1.17 | 1.75 | 2.04 | 2.6 | 0.48 | 0.22 | 1.91 | 0.07 | −0.24 | 0.53 | 0.567 |
| | | **Fry** | 1.49 | 1.11 | 0.6 | 1.35 | 1.83 | 2.47 | | | 0.42 | 2.18 | 0.13 | −0.26 | 0.651 | 0.337 |
| **AR8** | **Metavolcanic** | **Rf/φ** | 1.23 | 1.22 | 0.67 | 1 | 1.84 | 1.85 | … | … | 0.01 | 1.84 | 2 | −0.26 | 0.499 | 0.991 |
| | | **Fry** | 1.22 | 1.19 | 0.68 | 1.03 | 1.74 | 1.79 | | | 0.03 | 1.77 | 0.01 | −0.24 | 0.464 | 0.912 |
| **AR9** | **Metavolcanic** | **Rf/φ** | 1.28 | 1.25 | 0.63 | 1.03 | 1.99 | 2.05 | … | … | 0.03 | 2.02 | 0.01 | −0.3 | 0.574 | 0.927 |
| | | **Fry** | 1.94 | 1.04 | 0.49 | 1.87 | 2.1 | 3.93 | | | 0.79 | 2.97 | 0.27 | −0.32 | 0.968 | 0.086 |
| **AR10** | **Abt Schist** | **Rf/φ** | 1.26 | 1.25 | 0.64 | 1.01 | 1.96 | 1.97 | 2.3 | 0.64 | 0.01 | 1.96 | 0 | −0.29 | 0.551 | 0.983 |
| | | **Fry** | 1.36 | 1.06 | 0.69 | 1.28 | 1.54 | 1.98 | | | 0.52 | 1.82 | 0.11 | −0.19 | 0.488 | 0.27 |
| **AR11** | **Metavolcanic** | **Rf/φ** | 1.2 | 1.18 | 0.71 | 1.01 | 1.67 | 1.69 | … | … | 0.02 | 1.68 | 0.01 | −0.22 | 0.424 | 0.948 |
| | | **Fry** | 1.37 | 1.1 | 0.66 | 1.24 | 1.67 | 2.07 | | | 0.36 | 1.91 | 0.09 | −0.22 | 0.529 | 0.405 |
| **AR12** | **Abt Schist** | **Rf/φ** | 1.58 | 1.06 | 0.6 | 1.49 | 1.79 | 2.65 | 2.8 | 2.63 | 0.62 | 2.27 | 0.17 | −0.25 | 0.694 | 0.188 |
| | | **Fry** | 1.57 | 1.29 | 0.49 | 1.21 | 2.63 | 3.2 | | | 0.13 | 2.85 | 0.08 | −0.42 | 0.881 | 0.667 |
| **AR13** | **Metavolcanic** | **Rf/φ** | 1.19 | 1.14 | 0.74 | 1.04 | 1.53 | 1.6 | … | … | 0.08 | 1.58 | 0.02 | −0.18 | 0.367 | 0.815 |
| | | **Fry** | 1.18 | 1.03 | 0.82 | 1.15 | 1.24 | 1.43 | | | 0.63 | 1.4 | 0.06 | −0.09 | 0.256 | 0.209 |
| **AR14** | **Metavolcanic** | **Rf/φ** | 1.2 | 1.15 | 0.72 | 1.05 | 1.59 | 1.66 | … | … | 0.08 | 1.63 | 0.02 | −0.2 | 0.397 | 0.825 |
| | | **Fry** | 1.78 | 1.09 | 0.52 | 1.64 | 2.11 | 3.46 | | | 0.58 | 2.75 | 0.21 | −0.32 | 0.884 | 0.202 |
| **AR15** | **Abt Schist** | **Rf/φ** | 1.4 | 1.15 | 0.62 | 1.21 | 1.86 | 2.26 | 2.7 | 0.52 | 0.25 | 2.08 | 0.08 | −0.27 | 0.602 | 0.528 |
| | | **Fry** | 1.68 | 1.45 | 0.41 | 1.16 | 3.53 | 4.08 | | | 0.06 | 3.69 | 0.06 | −0.55 | 1.094 | 0.794 |
| **AR16** | **Metagrantic** | **Rf/φ** | 1.23 | 1.23 | 0.66 | 1.01 | 1.86 | 1.87 | … | … | 0.01 | 1.86 | 0 | −0.27 | 0.508 | 0.979 |
| | | **Fry** | 1.59 | 1.21 | 0.52 | 1.32 | 2.32 | 3.07 | | | 0.25 | 2.64 | 0.12 | −0.36 | 0.824 | 0.5 |
| **AR17** | **Metavolcanic** | **Rf/φ** | 1.51 | 1.11 | 0.6 | 1.36 | 1.86 | 2.53 | … | … | 0.43 | 2.22 | 0.14 | −0.27 | 0.669 | 0.331 |
| | | **Fry** | 1.28 | 1.28 | 0.61 | 1 | 2.11 | 2.12 | | | 0.01 | 2.11 | 0 | −0.32 | 0.61 | 0.992 |
| **AR18** | **Grantic gneisses** | **Rf/φ** | 1.32 | 1.2 | 0.63 | 1.11 | 1.89 | 2.09 | … | … | 0.12 | 2 | 0.04 | −0.28 | 0.566 | 0.729 |
| | | **Fry** | 1.6 | 1.16 | 0.54 | 1.37 | 2.17 | 2.98 | | | 0.32 | 2.54 | 0.14 | −0.34 | 0.794 | 0.419 |
| **AR19** | **Metavolcanic** | **Rf/φ** | 1.18 | 1.12 | 0.76 | 1.05 | 1.48 | 1.55 | … | … | 0.11 | 1.53 | 0.02 | −0.17 | 0.342 | 0.776 |
| | | **Fry** | 1.53 | 1.35 | 0.48 | 1.14 | 2.78 | 3.16 | | | 0.08 | 2.92 | 0.06 | −0.44 | 0.892 | 0.776 |
| **AR20** | **Metavolcanic** | **Rf/φ** | 1.26 | 1.17 | 0.68 | 1.07 | 1.72 | 1.85 | … | … | 0.1 | 1.79 | 0.03 | −0.24 | 0.475 | 0.773 |
| | | **Fry** | 2.97 | 0.85 | 0.39 | 3.48 | 2.16 | 7.51 | | | 2.13 | 4.64 | 0.54 | −0.33 | 1.439 | −0.236 |
| **AR21** | **Grantic gneisses** | **Rf/φ** | 1.27 | 1.24 | 0.63 | 1.02 | 1.97 | 2.01 | … | … | 0.02 | 1.99 | 0.01 | −0.29 | 0.563 | 0.937 |
| | | **Fry** | 1.85 | 1.02 | 0.62 | 1.55 | 1.64 | 2.55 | | | 0.87 | 2.19 | 0.19 | −0.21 | 0.661 | 0.056 |
| **AR22** | **Grantic gneisses** | **Rf/φ** | 1.25 | 1.22 | 0.66 | 1.03 | 1.86 | 1.9 | 2.4 | 2.6 | 0.03 | 1.88 | 0.01 | −0.27 | 0.515 | 0.922 |
| | | **Fry** | 1.84 | 1.14 | 0.48 | 1.6 | 2.41 | 3.86 | | | 0.43 | 3.01 | 0.21 | −0.38 | 0.969 | 0.3 |
| **AR23** | **Metagrantic** | **Rf/φ** | 1.24 | 1.17 | 0.69 | 1.06 | 1.7 | 1.79 | … | … | 0.08 | 1.75 | 0.02 | −0.23 | 0.456 | 0.814 |
| | | **Fry** | 1.66 | 1.03 | 0.59 | 1.62 | 1.75 | 2.84 | | | 0.83 | 2.37 | 0.21 | −0.24 | 0.738 | 0.072 |
| **AR24** | **Metavolcanic** | **Rf/φ** | 1.37 | 1.17 | 0.62 | 1.17 | 1.88 | 2.2 | … | … | 0.19 | 2.05 | 0.07 | −0.27 | 0.589 | 0.609 |
| | | **Fry** | 1.67 | 1.25 | 0.48 | 1.34 | 2.6 | 3.49 | | | 0.21 | 2.94 | 0.13 | −0.42 | 0.924 | 0.532 |
| **AR25** | **Grantic gneisses** | **Rf/φ** | 1.21 | 1.21 | 0.68 | 1 | 1.78 | 1.78 | 2.3 | 2.58 | 0.01 | 1.78 | 0 | −0.25 | 0.469 | 0.998 |
| | | **Fry** | 1.45 | 1.1 | 0.62 | 1.31 | 1.77 | 2.33 | | | 0.41 | 2.09 | 0.12 | −0.25 | 0.61 | 0.354 |
| **AR26** | **Grantic gneisses** | **Rf/φ** | 1.29 | 1.18 | 0.65 | 1.09 | 1.81 | 1.98 | … | … | 0.12 | 1.91 | 0.04 | −0.26 | 0.526 | 0.737 |
| | | **Fry** | 1.74 | 1.38 | 0.42 | 1.26 | 3.29 | 4.15 | | | 0.11 | 3.55 | 0.1 | −0.52 | 1.08 | 0.674 |
| **AR27** | **Grantic gneisses** | **Rf/φ** | 1.25 | 1.22 | 0.66 | 1.03 | 1.85 | 1.9 | 2.6 | 2.62 | 0.03 | 1.87 | 0.01 | −0.27 | 0.512 | 0.915 |
| | | **Fry** | 1.49 | 1.03 | 0.65 | 1.44 | 1.6 | 2.31 | | | 0.74 | 2.04 | 0.16 | −0.2 | 0.592 | 0.123 |
| **AR28** | **Grantic gneisses** | **Rf/φ** | 1.23 | 1.2 | 0.68 | 1.03 | 1.77 | 1.82 | … | … | 0.03 | 1.8 | 0.01 | −0.25 | 0.479 | 0.913 |
| | | **Fry** | 1.24 | 1.17 | 0.69 | 1.06 | 1.69 | 1.79 | | | 0.08 | 1.75 | 0.02 | −0.23 | 0.452 | 0.809 |
| **AR29** | **Metavolcanic** | **Rf/φ** | 1.28 | 1.13 | 0.69 | 1.14 | 1.63 | 1.85 | … | … | 0.23 | 1.77 | 0.06 | −0.21 | 0.46 | 0.573 |
| | | **Fry** | 1.27 | 1.15 | 0.68 | 1.11 | 1.69 | 1.87 | | | 0.16 | 1.79 | 0.04 | −0.23 | 0.473 | 0.673 |
| **AR30** | **Grantic gneisses** | **Rf/φ** | 1.3 | 1.26 | 0.61 | 1.03 | 2.04 | 2.11 | 2.6 | 2.64 | 0.03 | 2.08 | 0.01 | −0.31 | 0.597 | 0.917 |
| | | **Fry** | 1.45 | 0.95 | 0.72 | 1.53 | 1.32 | 2.01 | | | 1.67 | 1.84 | 0.18 | −0.12 | 0.497 | −0.213 |
| **AR31** | **Grantic gneisses** | **Rf/φ** | 1.19 | 1.17 | 0.72 | 1.02 | 1.63 | 1.66 | … | … | 0.03 | 1.65 | 0.01 | −0.21 | 0.408 | 0.924 |
| | | **Fry** | 1.66 | 1.15 | 0.52 | 1.44 | 2.22 | 3.19 | | | 0.36 | 2.65 | 0.16 | −0.35 | 0.839 | 0.371 |
| **AR32** | **Grantic gneisses** | **Rf/φ** | 1.33 | 1.15 | 0.66 | 1.15 | 1.76 | 2.03 | 2.5 | 2.6 | 0.2 | 1.91 | 0.06 | −0.24 | 0.528 | 0.593 |
| | | **Fry** | 1.29 | 1.28 | 0.6 | 1.01 | 2.12 | 2.14 | | | 0.01 | 2.13 | 0 | −0.33 | 0.617 | 0.98 |
| **AR33** | **Metagrantic** | **Rf/φ** | 1.18 | 1.15 | 0.73 | 1.03 | 1.57 | 1.61 | … | … | 0.05 | 1.6 | 0.01 | −0.2 | 0.381 | 0.893 |
| | | **Fry** | 1.26 | 1.06 | 0.74 | 1.18 | 1.43 | 1.69 | | | 0.43 | 1.61 | 0.07 | −0.16 | 0.38 | 0.356 |
| **AR34** | **Grantic gneisses** | **Rf/φ** | 1.33 | 1.19 | 0.63 | 1.12 | 1.87 | 2.09 | 2.4 | 0.52 | 0.13 | 1.99 | 0.05 | −0.27 | 0.562 | 0.702 |
| | | **Fry** | 1.66 | 1.39 | 0.43 | 1.2 | 3.2 | 3.82 | | | 0.09 | 3.39 | 0.08 | −0.51 | 1.03 | 0.734 |

Furthermore, the rocks represent monzodiorite, tonalite, granodiorite, alkali-feldspar granite, and gabbro intrusive rock units in the Al Amar area. Monzodiorite gneiss is often coarse sized crystals and exhibit holocrystalline, hypidiomorphic, poikilitic texture with metamorphism to gneiss rocks (Fig. 4A). Tonalite is often medium to coarse crystals size and display holocrystalline, hypidiomorphic, granitic texture with metamorphism to gneiss rocks (Fig. 4B). Alkali-feldsar granite is mainly of quartz, K-feldspar, with

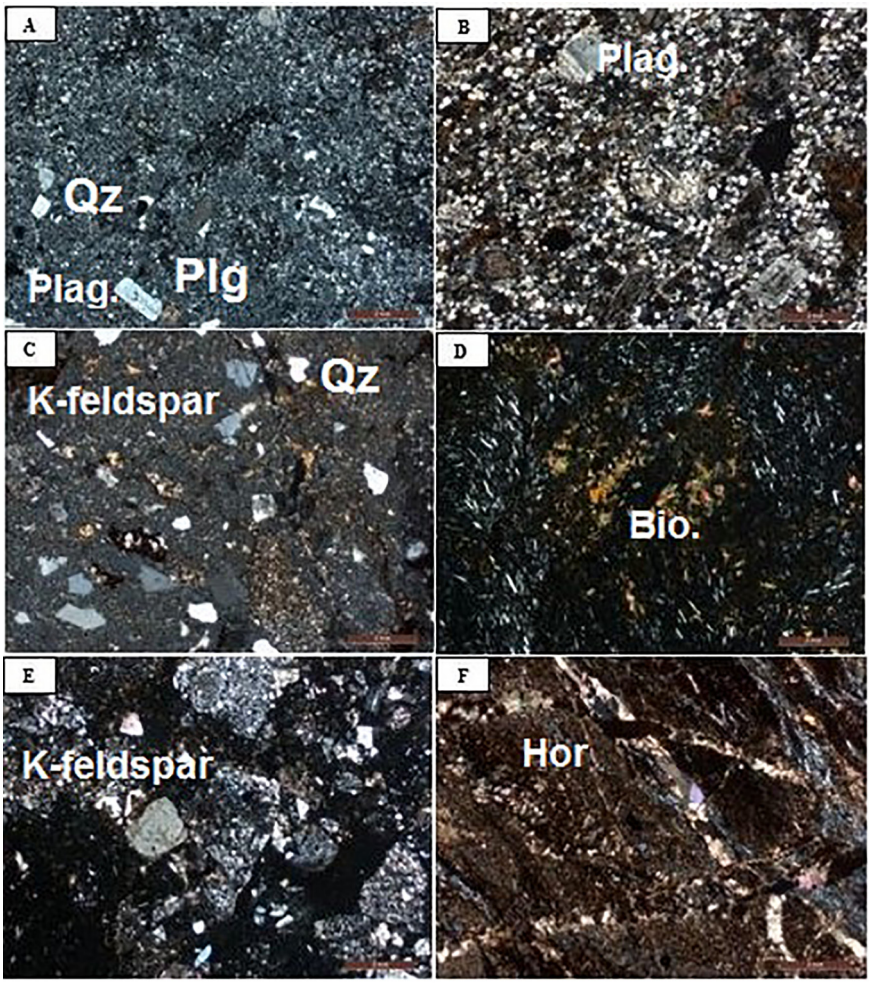


**Fig. 3.** Photomicrophotographs of metavolcanics rocks composed mainly showing (A) rhyolite, (B) dacite, (C) Ignimbrites, (D) andesite (E) pyroclastic and (F) Listwanites. Qz: Quartz, K-feldspar: Alkali feldspar, Plag: Plagioclase, Bio: Biotite, Pyr: Pyroxene and Hor: Hornblende.

a few plagioclase albite and biotite, with accessory minerals as iron oxides myrmekite texture (Fig. 4C). Granodiorte has quartz, plagioclase, K-feldspar, and biotite with a holocrystalline, hypidiomorphic, and poikilophitic texture (Fig. 4D). Gabbro is consists mainly of plagioclase, clinopyroxene and hornblende with minor biotite with highly fractured (Fig. 4E).

### *4.2. Microstructure investigation*

The X, Y, and Z axes are the primary directions of finite strain in the metavolcanics and granitoids gneisses rocks studied, which have well-defined planar and linear fabric components. Thin slices cut parallel to foliation (XY), normal to foliation and parallel to lineation (XZ), and normal to foliation and lineation (YZ) were studied microstructural. According to microstructure data, feldspar ductility occurs only at temperatures $\geq$ 450 °C during high-pressure metamorphism, along a significant thrust plane (Borghi, et al., 1996). The shear zone runs the length of the Al Amar suture, which display a north-trending shear zone with a sharp westward dip. NW–SE and N–S trends with a steeply falling plunge dominate the main structural properties of the investigated samples. In the NW–SE and E–W directions, the measured samples show elongate fabric with well-developed mineral lineation and gentle to medium dips.

The foliation for metavolcano-sedimentary, Abt schist, and granitic gneiss rocks along the Al Amar-Idsas fault is mainly NE–SW and E–W with slightly dipping foliation (Kassem and Hamimi 2014; Hamimi et al., 2015). Thick clastic sediments metamorphosed to the greenschist facies make up the Abt Formation. Metagreywacke, metasiltstone, and pelitic schists are some of the rocks that make up this group. The Al Amar-Idsas discontinuity is an N-trending fault/shear zone with a foliation that slopes sharply westward to vertical. The Abt schist is foliated moderately to strongly and well-oriented locally (Fig. 5). The Al Amar-Idsas fault on the western side, metavolcano-sedimentary rocks are primarily weakly to moderately deformed (Fig. 6). The granite gneiss unit is moderately to severely deformed, with well-defined foliation in certain areas (Fig. 7).

Quartz, plagioclase, alkali-feldspar, sericite, chlorite, calcite, and epidote were found in the study area's schist samples (orthoclase). The schist is mildly to severely distorted (Fig. 5). Vertical to subvertical foliation was seen in chlorite schist samples with oriented sericite, chlorite, epidote, and calcite grains, resulting in high to moderate deformation (Fig. 5A & B). Elongated feldspars (alkali-feldspar) and mafic minerals (chlorite and epidote) were also discovered with considerable elongation and deformation with high deformation (Fig. 5C & D). Quartz grains were rotated and elongated in certain instances.

Because of the strongly deformed, the Metavolcanics are exposed in the narrow western part of the Al Amar – Idsas suture and acquire a mostly N-S trend with moderately to strongly dipping subvertical foliations. In the Al Amar – Idsas fault,

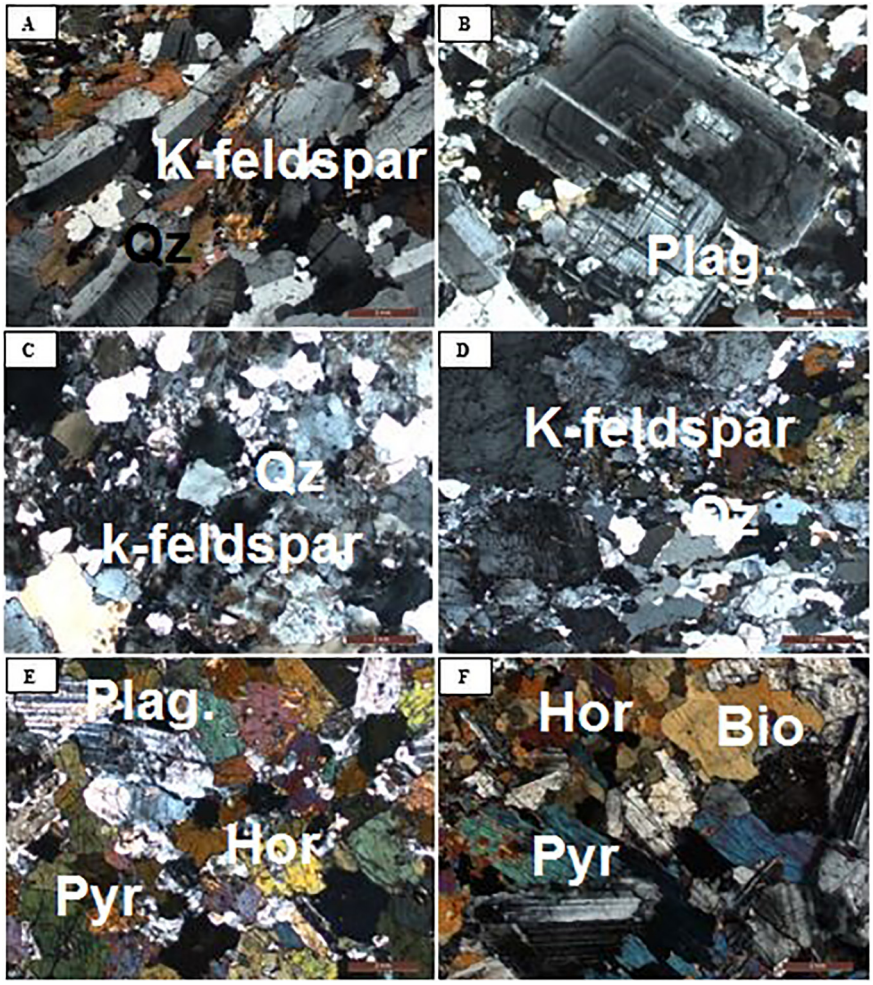


**Fig. 4.** Photomicrophotographs of granitiods rocks composed mainly showing (A) Monzodiorite, (B) Tonalite, (C) Alkali-feldspar granite, (D) Granodiorite, (E) and (F) Gabbro. Qz: Quartz, K-feldspar: Alkali feldspar, Plag: Plagioclase, Bio: Biotite, Pyr: Pyroxene and Hor: Hornblende.

deformation of fragments of a mélange of metavolcanic rocks rises as they approach the shear zone. Elongated felsic and mafic minerals are found in deformed samples. Felsic minerals include quartz and feldspar, while mafic minerals include hornblende and biotite (Fig. 6). Mineral lineation in certain samples is oriented to the northwest. Composition of minerals for moderately deformed volcanic rocks that they distorted sanidine, plagioclase (albite), and hornblende phenocrysts are contained in a crystalline groundmass with the same composition as certain quartz crystals in metadacite (Fig. 6A &B). In addition, the deformed volcanic rocks meta-andesite contain plagioclase and hornblende phenocrysts embedded in crystalline groundmass, as well as chlorite in the groundmass (Fig. 6C). Quartz, feldspars as sanidine, and occasionally plagioclase phenocrysts are surrounded muscovite and biotite associating in foliated groundmass with the same composition in severely deformed volcanic rocks known as meta-rhyolite (Fig. 6D). The granitoids gneiss has a well-developed granoblastic polygonal texture (Fig. 7) and is moderately to highly foliated. It shows a mild deformation increase towards the shear zone in the Al Amar–Idsas fault Zone in several areas. Elongated feldspars containing biotite and hornblende are seen in Fig. 7. In Fig. 7A & B, some granitic rocks have a medium to coarse crystals and are weakly foliated, whereas strong deformed quartz examples include elongated chlorite and hornblende (Fig. 7C & D).

### 4.3. Flow path analysis

The flow-path analysis determines the degree of non-coaxiality in a deformed rock by analyzing data from rotating rigid ellipsoids (Passchier, 1987). The Abt schist, metavolcano-sedimentary, and granitic gneiss samples that were obtained were measured. Rotated plagioclase, quartz, and hornblende porphyroclast, which indicate rigid clasts in the examined rocks, were given specific attention. The flow-path analysis was calculated the mean kinematic vorticity number (Wm). The vorticity study was carried out using Rigid Grain Net (RGN) methods (Kassem, 2012, 2014, 2015). Plagioclase and quartz, according to Passchier and Trouw (1995), have a comparable deformation behavior. The aspect ratio was the focus of the RGN approaches, which gave low and/or high values.

The flow-path analysis associated strains formed ductile-deformed feldspar porphyroclast may be credited with thrusting inspired deformation, according to these studies. The Al Amar–Idsas thrust fault occurs through Abt schist, metavolcano-sedimentary, and granitic gneiss, in the Al Amar region, according to our results. Kassem and Ring (2004) used petrography data to demonstrate the kind of rocks in samples with huge equal-sized plagioclases, quartz, and amphibole hornblende porphyroclast crystals for rotation analysis. This suggests that the time of

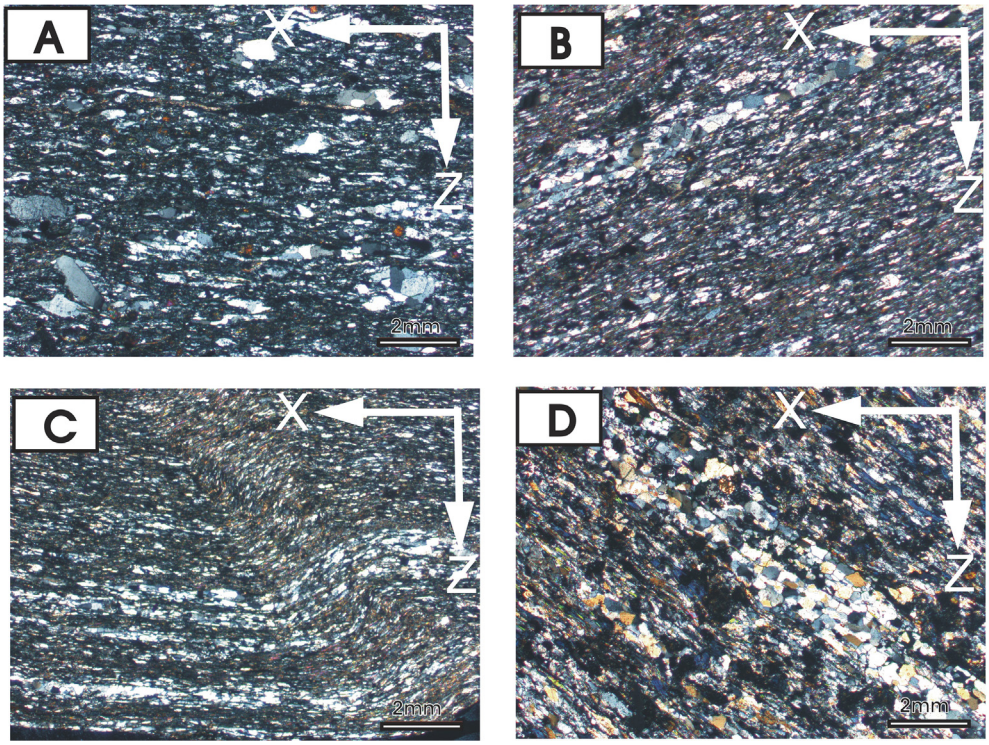


**Fig. 5.** A) Schist rocks show elongated feldspars with some rotated Qz, B) Schist rocks show strongly foliated minerals, C) Schist rocks show highly deformed with fold near the shear zones. D) Highly deformed schist rocks showing bedding.

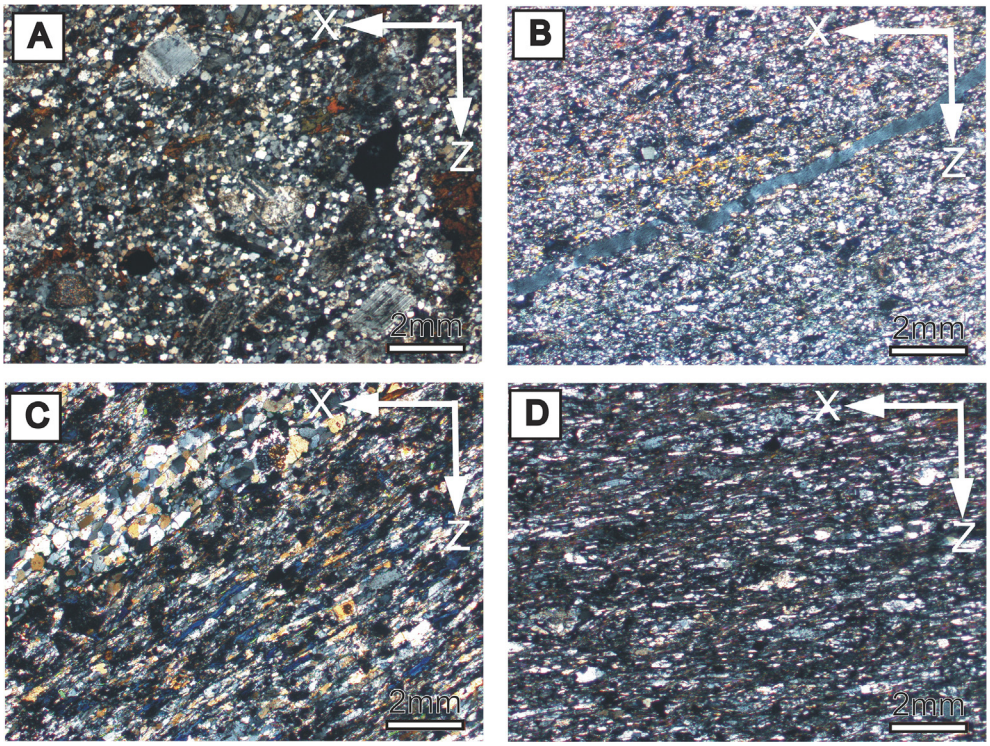


**Fig. 6.** A) Meta-andesite contains plagioclase, chlorite, epidote, hornblende, and alkali-feldspars, B) Meta-rhyolite includes quartz-rich, plagioclase, biotite grains, C) Foliated potash feldspar grains of schistose rocks. D) Highly deformed composed of quartz K-feldspar and biotite for metasedimentary rocks.

deformation during thrusting and intrusions is the buildup of brittle to semi-ductile deformation. In the Al Amar area, the structure is dominated by widespread and subhorizontal foliations from the primary metamorphic phase, which are practically sub parallel to the fault contacts (Lami et al., 2020). The flattening strain type indicates a deviation from simple shear deformation. A flow-path study was approved employing rotational rigid objects to identify the degree of non-coaxiality (Passchier, 1987).

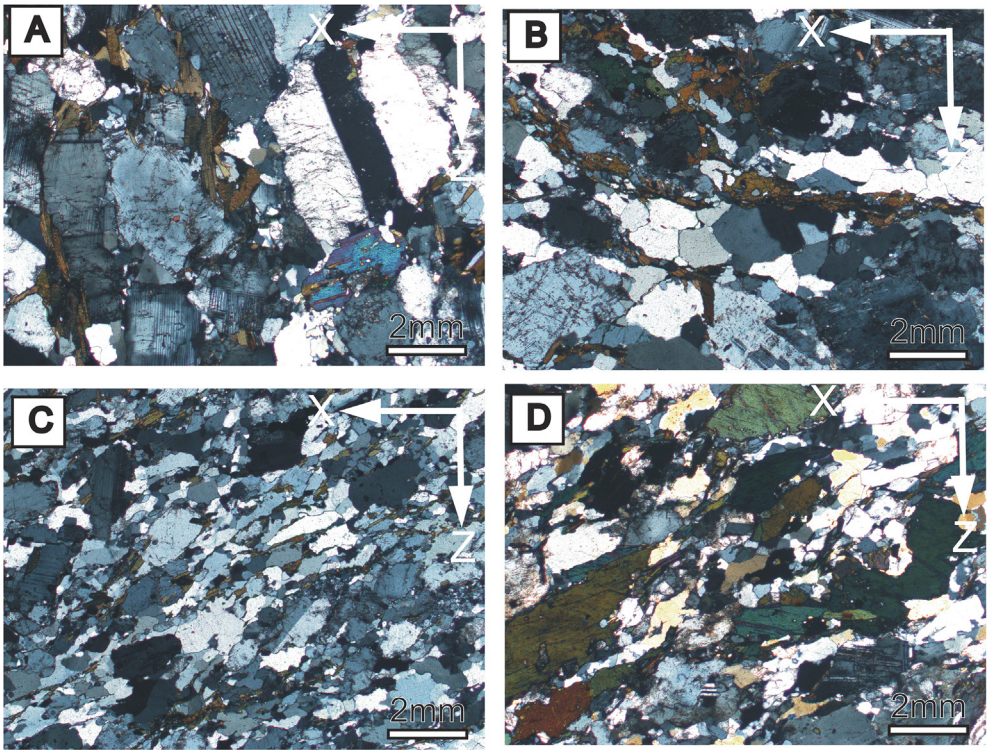


**Fig. 7.** A) Weakly deformed granitic gneisses rocks composed of quartz, plagioclase, K-feldspar, hornblende, and biotite, B) granitic gneisses show moderately deformed plagioclase, potash feldspar, and biotite grains, C) Elongated alkali-feldspar grains of granitic gneisses rocks. D) Highly deformed gneisses rocks.

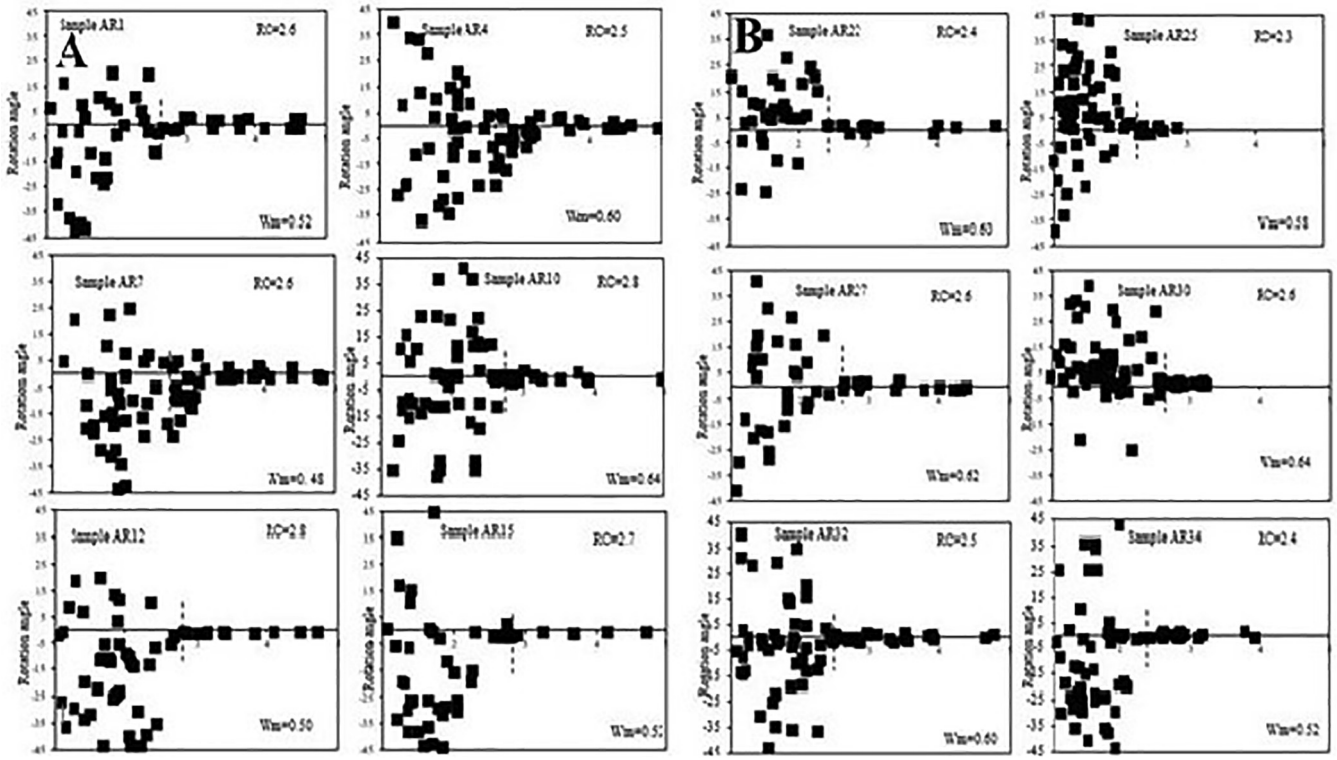


**Fig. 8.** A) The Passchier plot technique showing vorticity analyses for metavolcano-sedimentary and schist rocks; dashed line separates the measured samples, which displays a wide scatter from those with the stable orientation parallel to foliation; $R_C$ is shown in upper left. B) The Passchier plot technique showing vorticity analyses for gneisses rocks; dashed line separates the measured samples, which displays a wide scatter from those with the stable orientation parallel to foliation; $R_C$ is shown in upper left.

In the present work, our results is shown in Fig. 8A and 8B for high deformed samples for metavolcano-sedimentary and gneisses rocks respectively. The aspect ratio is low $\leq 45°$, and there is a dispersion across a large variety of orientations (Fig. 8A & B). In the studied samples, the critical values for RC vary 2.5 to −2.8 for metavolcano-sedimentary and schist (Fig. 8A) and 2.3–2.6 for

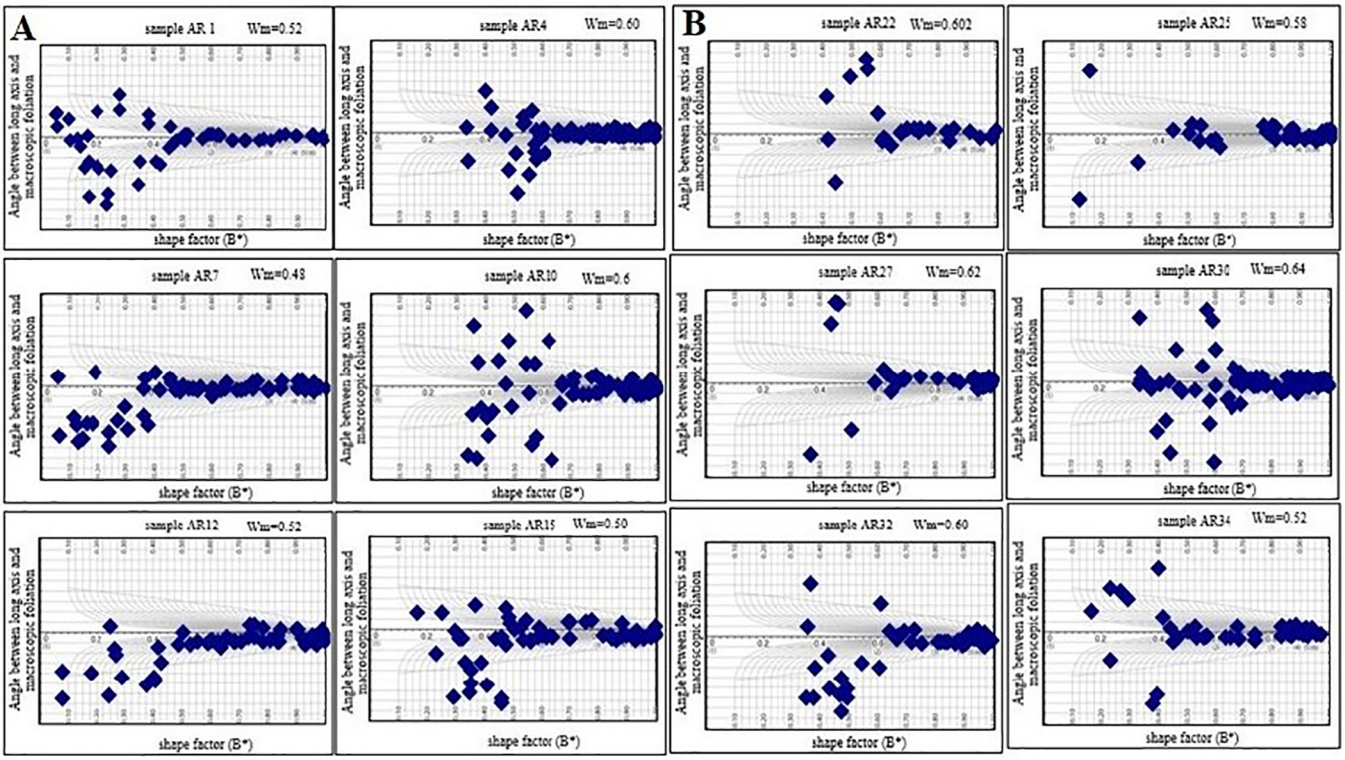


**Fig. 9.** A) The Rigid grain net (RGN) shows a plot of shape factor (B*) versus the angle between macroscopic foliation and long axis of clast for metavolcano-sedimentary and schist rocks. B) The Rigid grain net (RGN) shows a plot of shape factor (B*) versus the angle between macroscopic foliation and long axis of clast for gneisses rocks.

gneisses rocks (Fig. 8B). These values are viewed as the crucial RC values for distinguishing freely rotating porphyroclast from those that have stabilized during deformation. As a result, Wm varies from 0.48 to −0.64 for metavolcano-sedimentary and schist (Fig. 8A) and 0.52–0.64 for gneisses rocks (Fig. 8B). Plagioclases and alkali feldspar porphyroclast with aspect ratios of XZ sections are common in Al Amar area, which composed of gneisses and metavolcanics. Some examples have a low aspect ratio and are tightly packed, while others have a low aspect ratio and are inclined at angles close to 45 degrees to the mylonitic foliation. The angle of inclination reduces as the aspect ratio increases, as seen in Fig. 8A & B.

To compare the Passchier results and discover flow path analysis in shear zones, the RGN methodology is utilized. Fig. 9A and 9B depict the Wm values for RGN. These RC values are thought to be the most important in separating freely revolving porphyroclast from those that have stabilized during deformation. As a result, Wm for metavolcano-sedimentary and schist (Fig. 9A) ranges from 0.48 to 0.60, and 0.52–0.64 for gneisses rocks (Fig. 9B). The Wm values produced using both procedures are similar, indicating that the flow route analysis is valid (Fig. 9A and B). In metavolcanics, schist, and granitic gneisses rocks, these aspect ratio values are flattening strains consistent with vertical shortening normal to the main-phase foliation (Table 1).

## 5. Discussion

In the east of the Arabian Shield, the Al Amar-idsas suture runs parallel to the Al Amar Fault, which divides them. Its branching into a vast network of faults populated by interweaving quartz veins may be seen in the region's centre and west. It contains gold, pyrite, sphalerite, chalcopyrite, and chalcocite, among other minerals. The volcanic rocks consist of metamorphosed under greenschist facies interlayered with compositionally equivalent volcanoclastic and pyroclastic deposits. The volcanic lavas represent andesite, dacite, rhyodacite, rhyolite porphyry and rhyolite, while the volcanoclastic represent of pyroclastics cover the full series from coarse volcanic breccia to fine tuffs. While the granitoids represent Monzodiorite, tonalite, granodiorite and alkali-feldspar granite, in addition to gabbros complex.

The Al Amar group is surrounded on the eastern side by Al Amar fault, which are intermittent bands of volcano-sedimentary and volcanic rocks. Basalt may be found in a variety of locations in the Al Amar belt, including metamorphism converting into a split and basalt with schist in the alpine formation, as well as serpentinite, gabbro, and carbonate. We can see that most of these faults run northwest-southeast, in the same direction as the Red Sea, and that some others run northeast-southwest, parallel to the Najd faults system.

These study provides insight into petrography, finite strain analysis, flow-path analysis, and tectonic context. In the Al Amar area, we explore the genesis, tectonic history, and deformation variations of several types of rocks. The strain data describes the quality of constriction strain. In the present examined granitiods gneiss and metavolcanics rocks, strain measurements reveal oblate strain symmetry (see Table 1). It implies that simple shear drove the accumulation of ductile deformation during thrusting, with vertical shortening produced by a pure shear component. The sub-horizontal foliation in the thrusted Al Amar area of Ar Ryan terrane was induced by pure shear-related vertical shortening. At Wm = 0.64, pure and simple shear components have a non-linear relationship and contribute equally to total deformation (Law et al., 2004). The maximum strain ratio and the fabric skeleton of

quartz axis fabrics indicate typical kinematic vorticity values of 0.4–0.6. These data show a 60% pure shear component (Law et al., 2004), which dominates the ductile nappe emplacement associated deformation (Table 1).

In metavolcanics, schist and granitoids gneissose rocks, the results demonstrate oblate strain symmetry (constriction strain). This implies that the buildup of ductile to brittle deformation occurred during thrusting of the Ar Rayn region's metavolcanics sequences over the Ad Dawadimi region's granitoids rocks, followed by strike slip shear. We suppose that the Al Amar – Idsas fault was related to or followed by constriction strain, which might be a universal phenomenon (Al-Saleh and Kassem 2012; Kahal et al, 2019). The kinematic vorticity numbers of the metavolcanic samples are the same of granitoids in the Al Amar locality. Furthermore, the finite strain in metavolcanics, and schist rocks is on level with that seen in mylonitized granite rocks. As a result, it is proposed that the various lithologies emerge in the work. The same deformation affects metavolcanics, mylonitized granite, and schist rocks at the same time. The results reveal that the examined rocks in the Al Amar region were thrusted from a W/WSW stretching lineation during thrusting trend N/ENE, and accompanying kinematic markers tectonic transport from the record top to west.

## 6. Conclusions

Our results support that the kinematic vorticity number for metavolcanics and gneisses rocks revealed in the Ar Ryan terrane varies from 0.4 to 0.6, and along with the strain, data imply deviations from simple shear. The vorticity and strain analyses revealed that deformation in the region ranged from simple shear, most likely attributable to brittle imbrication, to ductile strain superimposed on the nappe structure under high pressure. Shear was used to accumulate ductile strain during over thrusting. It included a vertical shortening component that resulted in sub-horizontal foliation in the Ar Ryan terrane, which is sub-parallel to the nappe contacts with the underlying nappes. The similar deformation occurred in the exposed lithologies of the Ar Ryan terrane. This foliation occurred as the nappes were thrusted together, implying that nappe stacking was linked to vertical shortening. The tectonic transport direction in the Ar Ryan terrane was proposed to be west, according on observations.

## Declaration of Competing Interest

The authors declare that they have no known competing financial interests or personal relationships that could have appeared to influence the work reported in this paper.

## Acknowledgements

This Project was funded by the National Plan for Science, Technology and Innovation (MAARIFAH), King Abdulaziz City for Science and Technology, Kingdom of Saudi Arabia, Award Number (14-SPA154-02).

## References

Al-Saleh, A.M., Kassem, O.M.K., 2012. Microstructural, strain analysis and 40Ar/39Ar evidence for the origin of the Mizil gneiss dome, eastern Arabian Shield, Saudi Arabia. J. Afr. Earth Sc. 70, 24–35.

Borghi A., Sandrone R. 1996: Petrological constraints on the Alpine P–T history of the Internal Penninic Nappes of the Western Alps. In: Lombardo, B. (ed.) Studies on Metamorphic Rocks and Minerals of the western Alps. A Volume in Memory of Ugo Pognante. Bolletino Museo Regionale Scienze Nationale (Torino), 13, 329–359.

Doebrich, J.L., Zahony, S.G., Leavitt, J.D., Portacio, J.S., Siddiqui, A.A., Wooden, J.L., Fleck, R.J., Stein, H.J., 2004. Ad Duwayhi, Saudi Arabia: geology and geochronology of a Neoproterozoic intrusion-related gold system in the Arabian Shield. Econ. Geol. 99 (4), 713–741.

Doebrich, J., Al-Jehani, A., Siddiqui, A., Hayes, T., Saleh, Y., Wooden, J., Johnson, P., Kattan, F., Shaikan, B., Basahel, M., 2007a. Geology and mineral resources of the Ar Rayn terrane, eastern Arabian Shield, Kingdom of Saudi Arabia. Precambr. Res. 158, 17–50.

Doebrich, J.L., Al-Jehani, A.M., Siddiqui, A.A., Hayes, T.S., Wooden, J.L., Johnson, P.R., 2007b. Geology and metallogeny of the Ar Rayn terrane, eastern Arabian shield: Evolution of a Neoproterozoic continental-margin arc during assembly of Gondwana within the East African orogen. Precambr. Res. 158 (1-2), 17–50.

Fry, N., 1979. Random point distributions and strain measurement in rocks. Tectonophysics 60 (1-2), 89–105.

Ghosh, S.K., Ramberg, H., 1976. Reorientation of inclusions by combination of pure shear and simple shear. Tectonophysics 34 (1-2), 1–70.

Hamimi, Z., Kassem, O.M.K., El-Sabrouty, M.N., 2015. Application of kinematic vorticity techniques for mylonitized Rocks in Al Amar suture, eastern Arabian Shield, Saudi Arabia. Proc. Roy. Soc. Lond. Ser. A 49 (5), 439–450.

Johnson, P., Halverson, G., Kusky, T., Stern, R., Pease, V., 2013. Volcano sedimentary basins in the Arabian-Nubian Shield: Markers of Repeated Exhumation and Denudation in a Neoproterozoic Accretionary Orogen. Geosciences 3 (3), 389–445.

Jessup, M.J., Law, R.D., Searle, M.P., Frassi, C., 2007. The Rigid Grain Net (RGN): an alternative method for estimating mean kinematic vorticity number (Wm). J. Struct. Geol. 29, 411–421.

Kassem, O.M.K., Abd El Rahim, S.S., 2010. Finite strain analysis for the Metavolcanic-sedimentary rocks in the Gabel El-Mayet region, Central Eastern Desert, Egypt. J. Afr. Earth Sci. 58, 321–330.

Kahal, A.Y., El-Motaal, E.A., Kassem, O.M.K., Al Ghoreiby, A.H.R., 2019. Strain analysis and deformation history of Zalm area, Arabian Shield, Saudi Arabia. J. Afr. Earth Sci. 150, 441–450.

Kassem, O.M.K., 2011. Determining heterogeneous deformation for granitic rocks in the Northern thrust in Wadi Mubark belt, Eastern Desert, Egypt. Geotectonics 45, 244–254.

Kassem, O.M.K., 2012. Kinematic vorticity technique for porphyroclasts in the metamorphic rocks: An example from the Northern thrust in Wadi Mubarak belt, Eastern Desert, Egypt. Arab. J. Geosci. 5 (1), 159–167.

Kassem, O.M.K., Abd El Rahim, S.H., El Nashar, E.R., 2012. Strain analysis and microstructural evolution characteristic of Neoproterozoic rocks associations of Wadi El Falek, Centre Eastern Desert, Egypt. Geotectonics 46 (5), 379–388.

Kassem, O.M.K., 2014. Kinematic analysis of the Migif area in the Eastern Desert of Egypt. J. Afr. Earth Sci. 90, 136–149.

Kassem, O.M.K., Hamimi, Z., 2014. Application of finite strain technique for deformed lithologies in Al Amar suture, Eastern Arabian Shield. Open Geol. J. 8 (1), 97–106.

Kassem, O.M.K., Ibrahim, E.K.H., Lashin, A., Almutari, M., 2019a. Strain analysis and microstructural investigation of the Jabal Tays Ophiolite Complex, Eastern Arabian Shield. Saudi Arabia Geotecton. 53 (6), 752–764.

Kassem, O.M.K., Zakaria, H., Aboelkhair, H., Abdelhalim, A., Al-Gabali, M., 2019b. Microstructural study and strain analysis of deformed Neoproterozoic lithologies in Um Junud area, Northern Nubian Shield. Geotectonics 53 (1), 125–139.

Kassem, O.M.K., 2015. Strain analysis and deformation in the Tanumah Area, Arabian Shield, Saudi Arabia. Arab. J. Geosci. 8 (6), 4127–4138.

Kassem, O.M.K., Ring, U., 2004. Underplating-related finite-strain patterns in the Gran Paradiso massif, Western Alps, Italy: heterogeneous ductile strain superimposed on a nappe stack. J. Geol. Soc. 161 (5), 875–884.

Meert, J.G., Torsvik, T.H., 2003. The making and unmaking of a supercontinent: Rodinia revisited. Tectonophys 375, 261–288.

Passchier, C.W., 1987. Stable positions of rigid objects in non-coaxial flow: a study in vorticity analysis. J. Struct. Geol. 9, 679–690.

Passchier, C.W., 1990. Reconstruction of deformation and flow parameters from deformed vein sets. Tectonophysics 180, 185–199.

Passchier, C.W., Trouw, R.A., 1995. Microtectonics. Springer, Berlin Heidelberg New York.

Passchier, C.W., Urai, J.L., 1988. Vorticity and strain analysis using Mohr diagrams. J. Struct. Geol. 10, 755–763.

Lami, A.N.M., Osama, M.K.K., Al Bassam, A.M.M., 2020. Finite strain analysis for deformed Neoproterozoic rock associations of the Al Amar fault zone, Eastern Arabian Shield, Saudi Arabia, Arabian Journal of Geosciences, 13:272–288.Le Bel, L., Laval, M., 1986: Felsic plutonism in the Al Amar-Idsas area, Kingdom of Saudi Arabia. J. Afr. Earth Sci. 4, 87–98.

Ring, U., Kassem, O.M.K., 2007. the nappe rule: why does it work? J. Geol. Soc. 164 (6), 1109–1112.

Ramsay, J.G., 1967. Folding and Fracturing of Rocks. McGraw Hill, New York.

Ramsay, J.G., Huber, M.I., 1983. The Techniques of Modern Structural Geology, vol. 1. Academic, London.

Law, R.D, Searle, M.P., Simpson, R.L. 2004. Strain, deformation temperatures and velocity of flow at the top of the Greater Himalayan Slab, Everest Massif, Tibet, J. Geol. Soc. (London, U. K.) 161, 305–320.

Stern, R.J., 1994. Arc assembly and continental collision in the Neoproterozoic East African Orogen: implications for the consolidation of Gondwanaland. Ann. Rev. Plan. Sci. 22 (1), 319–351.

Simpson, C., De Paor, D.G., 1993. Strain and kinematic analysis in general shear zones. J. Struct. Geol. 15 (1), 1–20.

Ring, U., Brandon, M.T. 1999. Deformation and mass loss in the Franciscan subduction complex: Implications for exhumation processes in accretionary wedges," in Exhumation processes: Normal Faulting, Ductile Flow, and Erosion, Vol. 154 of Geol. Soc. London, Spec. Publ., Ed. by U. Ring, M. T. Brandon, G. S. Lister, and S. D. Willett (London, 1999), pp. 55–86.

Vaslet, D., Delfour, J., Manivit, J., Le Nindre, Y., Brosse, J., and Fourniguet, J., 1983: Geologic map of the Wadi Ar Rayn quadrangle, sheet 23 H, Kingdom of Saudi Arabia: Saudi Arabian Deputy Ministry for Mineral Resources, Jeddah, Geosciences Map, GM-63A.

Zhang, Q., Fossen, H., 2020. The dilemma of asymmetric porphyroclast systems and sense of shear. J. Struct. Geol. 130, 103893.